Atmos. Chem. Phys., 23, 6113–6126, 2023
https://doi.org/10.5194/acp-23-6113-2023

Atmospheric Chemistry and Physics
Open Access
EGU

Simultaneous formation of sulfate and nitrate via co-uptake of SO_2 and NO_2 by aqueous NaCl droplets: combined effect of nitrate photolysis and chlorine chemistry

Ruifeng Zhang[1,2] **and Chak Keung Chan**[1,2,3,a]

[1]School of Energy and Environment, City University of Hong Kong, Tat Chee Avenue, Kowloon 999077, Hong Kong SAR, China
[2]Shenzhen Research Institute, City University of Hong Kong, Shenzhen 518057, China
[3]Low-Carbon and Climate Impact Research Centre, City University of Hong Kong, Tat Chee Avenue, Kowloon 999077, Hong Kong SAR, China
[a]current address: Division of Physical Science and Engineering, King Abdullah University of Science and Technology, Thuwal, 23955-6900, Saudi Arabia

Correspondence: Chak Keung Chan (chak.chan@kaust.edu.sa, chak.k.chan@cityu.edu.hk) and Ruifeng Zhang (ruifengzhang.cn@gmail.com)

Received: 10 February 2023 – Discussion started: 14 February 2023
Revised: 14 April 2023 – Accepted: 8 May 2023 – Published: 5 June 2023

Abstract. SO_2 and NO_2 are the critical precursors in forming sulfate and nitrate in ambient particles. We studied the mechanism of sulfate and nitrate formation during the co-uptake of NO_2 and SO_2 into NaCl droplets at different RHs under irradiation and dark conditions. A significant formation of nitrate attributable to NO_2 hydrolysis was observed during the NO_2 uptake under all conditions, and its formation rate increases with decreasing RH. The averaged NO_2 uptake coefficient, γ_{NO_2}, from the unary uptake of NO_2 into NaCl droplets under dark conditions is 1.6×10^{-5}, 1.9×10^{-5}, and 3.0×10^{-5} at 80 %, 70 %, and 60 % RH, respectively. Chloride photolysis and nitrate photolysis play a crucial role in sulfate formation during the co-uptake. Nitrate photolysis generates reactive species (e.g., OH radicals, NO_2, and N(III)) that directly react with S(IV) to produce sulfate. The OH radicals generated from nitrate photolysis can also react with chloride ions to form reactive chlorine species and then sulfate. To parameterize the role of nitrate photolysis and chloride photolysis in forming sulfate, the SO_2 uptake coefficient, γ_{SO_2}, as a function of the nitrate photolysis rate, $P_{NO_3^-}$ ($j_{NO_3^-} \times [NO_3^-]$), and chloride photolysis rate, P_{Cl^-} ($j_{Cl^-} \times [Cl^-]$), was derived as $\gamma_{SO_2} = 0.41 \times P_{NO_3^-} + 0.34 \times P_{Cl^-}$. Our findings open up new perspectives on the formation of secondary aerosol from the combined effect of nitrate photolysis and chlorine chemistry.

1 Introduction

Sea salt aerosol (SSA) is one of the most abundant natural atmospheric particles in coastal environments (Chan and Yao, 2008). Mainly composed of NaCl, it is generated from bursting bubbles during whitecaps in the open ocean. In the atmosphere, fresh SSA can serve as reactive surfaces for the uptake of acidic gases such as SO_2, NO_2, and organic acids, followed by the release of HCl in the so-called "chloride depletion" reaction (Laskin et al., 2012; Yao et al., 2003). In the marine area or coastal region, the air pollutants, such as SO_2 and NO_2, emitted by substantial shipping emissions have attracted worldwide attention (Corbett et al., 2007; Zhang et al., 2019). These processes transform fresh SSA

into aged SSA containing $NaNO_3$, Na_2SO_4, and organic salts (Yao and Zhang, 2012). In addition, chloride ions in the particles can also undergo reactions to produce a series of reactive chlorine species (e.g., $Cl^{\bullet}$ and $Cl_2^{\bullet-}$) that can significantly increase atmospheric oxidative capacity and formation of secondary pollutants (Wang and Ruiz, 2017; Y. Wang et al., 2020; Young et al., 2014; Gen et al., 2020). In this study, we explore the co-uptake of SO_2 and NO_2 by NaCl droplets in producing sulfate and nitrate under irradiation and dark conditions.

Sulfate is one of the most abundant inorganic components in ambient particulate matter (Chan and Yao, 2008). Although SO_2 emissions have been drastically reduced in China in the past decade (Zheng et al., 2018), the concentration of sulfate is still at a high level. On the other hand, NO_2 concentrations have not been reduced as significantly as SO_2 (Zheng et al., 2018). Due to the ubiquitous co-existence of SO_2 and NO_2 in the atmosphere, numerous experimental (Liu and Abbatt, 2021; Wang et al., 2016; Cheng et al., 2016; Ge et al., 2019; Li et al., 2018a; J. Wang et al., 2020) and theoretical (Yang et al., 2019; Tang and Li, 2021) studies have examined the role of NO_2 in the oxidation of SO_2 in/on aqueous particles and mineral dust surface. In aqueous particles, dissolved NO_2 reacts with S(IV) ($SO_2 + HSO_3^- + SO_3^{2-}$) to produce sulfate, S(VI):

$$\mathrm{S(IV)} + 2\mathrm{NO_2(aq)} + \mathrm{H_2O} \rightarrow \mathrm{S(VI)} + 2\mathrm{H^+} + 2\mathrm{N(III)(aq)}. \quad \text{(R1)}$$

N(III) (NO_2^- / HONO) is produced as a by-product. In addition, gaseous NO_2 partitions into the aqueous phase and undergoes hydrolysis (disproportionation) to produce nitrate and N(III) (Reaction R2). It has been reported that N(III) can also react with S(IV) to produce sulfate (J. Wang et al., 2020; Gen et al., 2019a).

$$\mathrm{NO_2(aq)} + \mathrm{NO_2(aq)} + \mathrm{H_2O} \rightarrow \mathrm{N(III)(aq)} + \mathrm{NO_3^-(aq)} + 2\mathrm{H^+} \quad \text{(R2)}$$

While sulfate formation via NO_2 oxidation under dark conditions has been widely reported, studies investigating the mechanisms of such processes under irradiation are scarce. Li et al. suggested that N(III) generated from the hydrolysis of NO_2 can be photolyzed to produce OH radicals that can further react with S(IV) to form sulfate (Li et al., 2018a). Our earlier works (Gen et al., 2019a, b; Zhang et al., 2020) reported effective SO_2 oxidation mediated by particulate nitrate photolysis; that is, oxidants (e.g., OH radicals, NO_2, and N(III)) generated from particulate nitrate photolysis react with S(IV) to yield sulfate.

The relative contribution of nitrate to PM pollution has increased in the past few years (Lin et al., 2020; Xie et al., 2020; Fu et al., 2020). NO_2 is a key precursor of nitrate, and its role in forming nitrate has been well-documented. Prior studies have reported the major formation pathways via gas-phase oxidation and subsequent gas–particle partitioning to produce nitrate (Seinfeld and Pandis, 2006; Alexander et al., 2009), for instance, gas-phase oxidation of NO_2 by OH radicals to form nitric acid. In addition, free nitrate radicals (NO_3), produced from the reaction of NO_2 with O_3, can also react with NO_2 to produce dinitrogen pentoxide (N_2O_5), which partitions into particles to form nitrate. Besides, the heterogeneous uptake of NO_2 onto aqueous particles, mineral dust, and urban grime with subsequent hydrolysis (Reaction R2) to form nitrate has been reported (Yu et al., 2021; Dyson et al., 2021; Martins-Costa et al., 2020; Xu et al., 2019; Liu et al., 2019; Tan et al., 2016). The reactive uptake coefficient of NO_2, γ_{NO_2}, is a crucial parameter controlling heterogeneous processes on the aerosol surface. The contribution of NO_2 hydrolysis in forming nitrate from chemical transport models typically varies widely due to the significant uncertainties in γ_{NO_2} (Xie et al., 2022; Qiu et al., 2019b; Chan et al., 2021). On the other hand, because much attention to R2 is principally due to the failure of the current atmospheric model to predict observed concentrations of HONO and OH radicals (Liu et al., 2019; Pandit et al., 2021; Xu et al., 2019; Li et al., 2018b), the nitrate formation rate via NO_2 uptake and hydrolysis (Reaction R2) under various conditions, such as the presence of SO_2 and/or irradiation, has not been adequately addressed.

In this work, we studied sulfate and nitrate formation during the co-uptake of SO_2 and NO_2 by NaCl droplets under dark and irradiation conditions (Fig. 1). We reported an enhanced sulfate production rate during co-uptake of SO_2 and NO_2 under irradiation compared to dark conditions. In addition, a significant amount of nitrate was formed under all conditions examined. A kinetic model was constructed to study the mechanisms of sulfate and nitrate formation. We found that the interaction between nitrate photolysis and chlorine chemistry plays an important role in sulfate formation. The factors affecting the sulfate and nitrate formation rates were also discussed.

2 Method and materials

2.1 Materials

Aqueous stock solutions of sodium chloride (NaCl; 99.8 %, Unichem), sodium nitrate ($NaNO_3$; > 99 %, Acros Organics), sodium sulfate (Na_2SO_4; > 99 %, Acros Organics), and ammonium sulfate ($(NH_4)_2SO_4$; > 99 %, VWR Chemicals BDH) were prepared by dissolving corresponding salts into ultrapure water. The stock solution was atomized to generate droplets by a droplet generator (MicroFab Technologies, serial no. JD5-1008), and individual droplets of a diameter of (57 ± 2) µm were collected on a transparent hydrophobic substrate (model 5793, YSI Inc.) in a flow cell. The deposited droplets were equilibrated for ~ 30 min at a given RH before each reactive uptake experiment. Although the droplets used in this study are larger than ambient particles, we analyzed the kinetic data using uptake coefficients, which take size effects into consideration. The

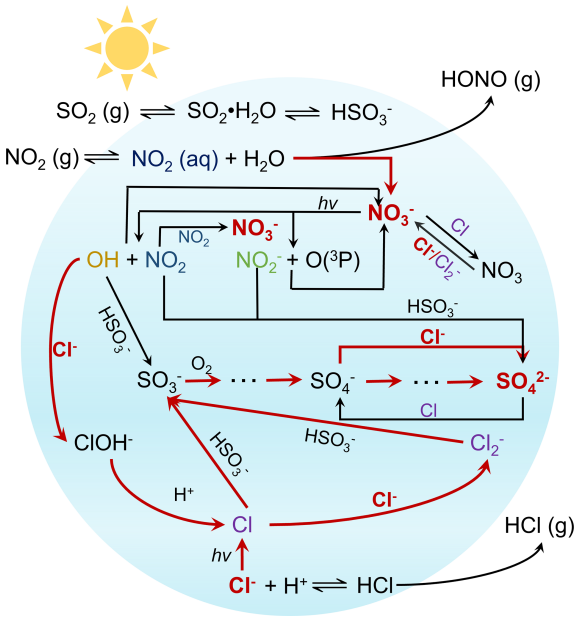

Figure 1. The sulfate and nitrate formation mechanisms during the co-uptake of NO_2 and SO_2 into NaCl droplets under irradiation. The red arrows highlight the role of enhanced chlorine chemistry triggered by OH radicals produced from nitrate photolysis in forming sulfate.

irradiation experiments were initiated using a xenon lamp (model 6258, ozone-free xenon lamp, 300 W, Newport) equipped with a long-pass filter (20CGA 305 nm cut-on filter, Newport) to eliminate light below 300 nm. The averaged initial photon fluxes at 280 to 420 nm received by droplets were $\sim 4.0 \times 10^{16}$ photons cm^{-2} s^{-1} using 2-nitrobenzaldehyde as a chemical actinometer (Gen et al., 2020, 2021).

2.2 Reactive uptake experiments and in situ Raman characterization

The reactive uptake of SO_2 and NO_2 into NaCl droplets experiments was performed using a Raman microscope/flow cell setup (Fig. S1 in the Supplement), described in detail in our previous studies (Gen et al., 2019a, b; Zhang et al., 2020, 2021, 2022; Gen et al., 2021, 2020). Here, we give a brief description. The reactive uptake experiments were performed with SO_2 and NO_2 concentrations of ~ 6.5 and ~ 10 ppm, respectively, under controlled relative humidity (RH) and light/dark conditions. The RH in the flow cell was controlled by adjusting wet and dry synthetic airflow rates. We studied the uptake process and its subsequent reactions by in situ characterization of the variation in particle composition by Raman spectroscopy (EnSpectr R532, EnSpectr). The Raman shifts at ~ 980, ~ 1050, and ~ 3400 cm^{-1} are assigned to $v(SO_4^{2-})$, $v(NO_3^-)$, and $v(OH)_{water}$, respectively. The change in concentration of $[SO_4^{2-}]$ and $[NO_3^-]$ in droplets was quantified by using established calibration curves (Fig. S2). The reacted droplets were dissolved in ~ 1 mL ultrapure water, followed by ion chromatograph analysis (IC analysis) with an IonPac AS15 analytical column, an AG15 guard column, and a conductivity detector. In addition, the droplet pH was measured by colorimetric analysis of images collected immediately after collection on pH indicator paper (Craig et al., 2018).

2.3 Kinetic simulations

A kinetic model was constructed in a chemical kinetics simulation package (FACSIMILE) to better understand reaction mechanisms. The reactions listed in Table S1 were used in the kinetic model. The model simulation results are shown in Fig. S3. In general, the agreement between the observed and predicted sulfate and nitrate concentrations was good. The initial chloride concentrations at different RHs were estimated based on the Extended Aerosol Inorganics Model (E-AIM) (Clegg et al., 1998). Note that chloride loss may occur in the form of HCl at equilibrium; hence, the corrected chloride concentrations based on IC analysis were used as input in the model (Table S2). We performed experiments with unary uptake of NO_2 into NaCl droplets under dark conditions to monitor the chloride depletion due to the increased acidity. As shown in Fig. S4, the molar ratio of Cl^- to Na^+, $n(Cl^-)/n(Na^+)$, decreased during the reaction. We simulate the evaporation of HCl based on the IC results to obtain the depletion rate of Cl^- ($Cl^- \rightarrow$ HCl (g)), which was also incorporated into the kinetic model in all conditions. The nitrate photolysis rate constant, $j_{NO_3^-}$, and the chloride photolysis rate constant of $Cl^- + h\nu \rightarrow Cl^\bullet$, j_{Cl^-}, were used as the fitting parameters to reproduce the observed changes in sulfate and nitrate concentrations. The fitted $j_{NO_3^-}$ and j_{Cl^-} are on the order of 10^{-6} and 10^{-7} s^{-1} (Table S3), respectively, which fall in the range reported in the literature (Gen et al., 2019a; Zhang et al., 2020; Kalmár et al., 2014; Ye et al., 2017). In addition, the effective Henry's law constant of NO_2 and SO_2, denoted as $H^*_{NO_2}$ and $H^*_{SO_2}$, respectively, may vary due to the reactions in the droplets. Equations of $H^*_{NO_2}$ and $H^*_{SO_2}$ as a function of time were established based on the observed time profiles of nitrate and sulfate (Text S1), which were incorporated in the model simulation.

3 Results and discussions

3.1 Mechanisms of sulfate formation under irradiation

As displayed in Fig. 2a, no observable sulfate formation was found during the co-uptake of NO_2 and SO_2 into aqueous NaCl droplets at 80 % RH under dark conditions, indicating that direct aqueous oxidation of S(IV) by NO_2 (Reaction R1) might not make a significant contribution to sulfate in the present study. The same was observed at

all RH values (Fig. 3a). This contrasts with some prior studies on significant sulfate formation from the oxidation of S(IV) by NO_2 during the polluted period (Wang et al., 2016; J. Wang et al., 2020; Liu and Abbatt, 2021). The negligible sulfate formation in our study may be due to the rapid drop in pH (Fig. S5). Specifically, NO_2 uptake and subsequent hydrolysis release H^+ (Reaction R2), increasing particle acidity, which limits the dissolution of SO_2 (Seinfeld and Pandis, 2006). Figure S5 shows pH decreases to about 2 within 240 min due to the NO_2 hydrolysis.

The co-uptake of SO_2 and NO_2 under irradiation gave an enhanced sulfate formation rate ($\sim 2.7 \times 10^{-6}\,M\,s^{-1}$; Fig. 2a) compared to that under dark conditions at 80 % RH, which suggests there are additional photochemical pathways to sulfate production. Several pathways of sulfate formation might explain these observations. First, $O(^3P)$ atoms generated from NO_2 (g) photolysis ($\lambda \leq 420$ nm) can react with O_2 to form O_3 (g) in air ($O_2 + O(^3P) \rightarrow O_3$) (Trebs et al., 2009; Gardner et al., 1987). Dissolved O_3 in aqueous particles can react with S(IV) to form sulfate (Seinfeld and Pandis, 2006). However, our open-system experiments with a continuous airflow ($\sim 0.5\,L\,min^{-1}$) would have removed the formed O_3 efficiently. Second, reactive chlorine species (e.g., $Cl^\bullet$ and $Cl_2^{\bullet-}$) can be formed by photoinduced electron transfer from chloride ions, denoted as "chloride photolysis" (CP for short) hereafter (Zhang and Parker, 2018; Grossweiner and Matheson, 1957; Kalmár et al., 2014). These chlorine species can react with S(IV) to produce sulfate (Table S1) (Zhang et al., 2020). As shown in Fig. 2a, the formation of sulfate ($\sim 1.3 \times 10^{-6}\,M\,s^{-1}$) was observed during the unary uptake of SO_2 into NaCl droplets under irradiation. No sulfate peak was detected in NaCl droplets without irradiation in the presence of SO_2 alone (Fig. 2a). In addition, lower light intensity yields a slower sulfate formation from the unary uptake of SO_2 (Fig. S6 and Table S4), further confirming that the chloride photolysis process can drive the sulfate formation. It should be noted that only chloride-photolysis-driven sulfate production cannot explain the observed higher sulfate production rate during the co-uptake (Fig. 2a). Third, N(III) ($HONO / NO_2^-$), produced from the reaction of NO_2 with S(IV) (Reaction R1) (Tang and Li, 2021; Liu and Abbatt, 2021; J. Wang et al., 2020; Ge et al., 2019) and NO_2 hydrolysis (Reaction R2) (Yabushita et al., 2009), can directly react with HSO_3^- to produce sulfate (J. Wang et al., 2020) or indirectly undergo photolysis to produce OH radicals that further promote sulfate formation (Seinfeld and Pandis, 2006). Interestingly, no NO_2^- Raman peak was observed in all experiments (Fig. S7). IC analysis also confirmed negligible NO_2^- in the reacted droplets (Fig. S8). We postulated that HONO from the protonation of NO_2^- partitions into the gas phase at low pH (Fig. S5) and can be removed rapidly because of the open flow cell system. Figure S5 shows that the droplet pH decreases below the pKa of NO_2^- / HONO (~ 3.2) (Arakaki et al., 1999) within 240 min due to the NO_2 hydrolysis. Li et al. (2018a) found that more than 95 % of NO_2 was hydrolyzed to form HONO and nitrate at the surface of aqueous sodium sulfite microjets (Li et al., 2018a). The effective mass transfer of HONO between particles and gas makes the accumulation of nitrite inside particles negligible. Thus, $HONO / NO_2^-$ is not expected to have significantly contributed to the sulfate production.

On the contrary, significant nitrate production was found during the co-uptake under both light and dark conditions (Fig. 4a). Our previous works (Gen et al., 2019a, b; Zhang et al., 2020) reported that particulate nitrate photolysis (NP for short) could effectively promote the oxidation of SO_2 to form sulfate. We attributed the further enhanced sulfate production during the co-uptake compared to the unary uptake of SO_2 to nitrate photolysis (Fig. 2a). First, the reactive species (e.g., OH, NO_2, and N(III)) produced from nitrate photolysis (denoted as "NP + ONN" reactions) (i.e., SR1 in Table S1) can directly react with S(IV) to form sulfate, denoted as the $[SO_4^{2-}]_{NP+ONN}$ pathway (Gen et al., 2019b, a). Second, the OH radicals generated from nitrate photolysis can react with Cl^- to yield the reactive chlorine species (e.g., $Cl^\bullet$ and $Cl_2^{\bullet-}$, denoted as "NP + Cl" reactions) (i.e., SR41, SR42, and SR43 in Table S1) that could further enhance sulfate production, denoted as the $[SO_4^{2-}]_{NP+Cl}$ pathway. Note that $[SO_4^{2-}]_{NP+Cl}$ pathway does not require chloride photolysis. In addition, we previously reported enhanced sulfate production from the halide-induced enhancement of nitrate photolysis by attracting more nitrate towards the interface, where an incomplete solvent cage leads to an increase in the quantum yield of oxidants from nitrate photolysis (Zhang et al., 2020). Such an effect might be embedded in the two processes mentioned above, especially at $[Cl^-] / [NO_3^-] \leq 0.2$, as proposed in our earlier work (Zhang et al., 2020). However, the model-predicted $[Cl^-] / [NO_3^-]$ values at all studied RHs were higher than 0.2 in this study; hence the halide-induced enhancement of nitrate photolysis is minor within the simulation timescale in the kinetic model. The contribution of different pathways to sulfate production will be discussed later. The role of nitrate photolysis in sulfate formation, $[SO_4^{2-}]_{NP}$, hereafter refers to the sum of $[SO_4^{2-}]_{NP+ONN}$ and $[SO_4^{2-}]_{NP+Cl}$ pathways, except when stated otherwise.

We used the kinetic model to simulate the time series of sulfate concentration during the co-uptake of NO_2 and SO_2 under irradiation at 80 % RH to understand the sulfate formation mechanisms. The contributions of chloride photolysis, $[SO_4^{2-}]_{CP}$, and nitrate photolysis (i.e., $[SO_4^{2-}]_{NP} = [SO_4^{2-}]_{NP+ONN} + [SO_4^{2-}]_{NP+Cl}$) to sulfate production were evaluated in the kinetic model. Figure 2b shows that the $[SO_4^{2-}]_{CP}$ pathway dominates over the $[SO_4^{2-}]_{NP}$ before ~ 1200 min, due to the high concentration of chloride. The contribution of the $[SO_4^{2-}]_{CP}$ pathway to total sulfate production continuously decreases. In contrast, the fraction of sulfate concentration generated from the

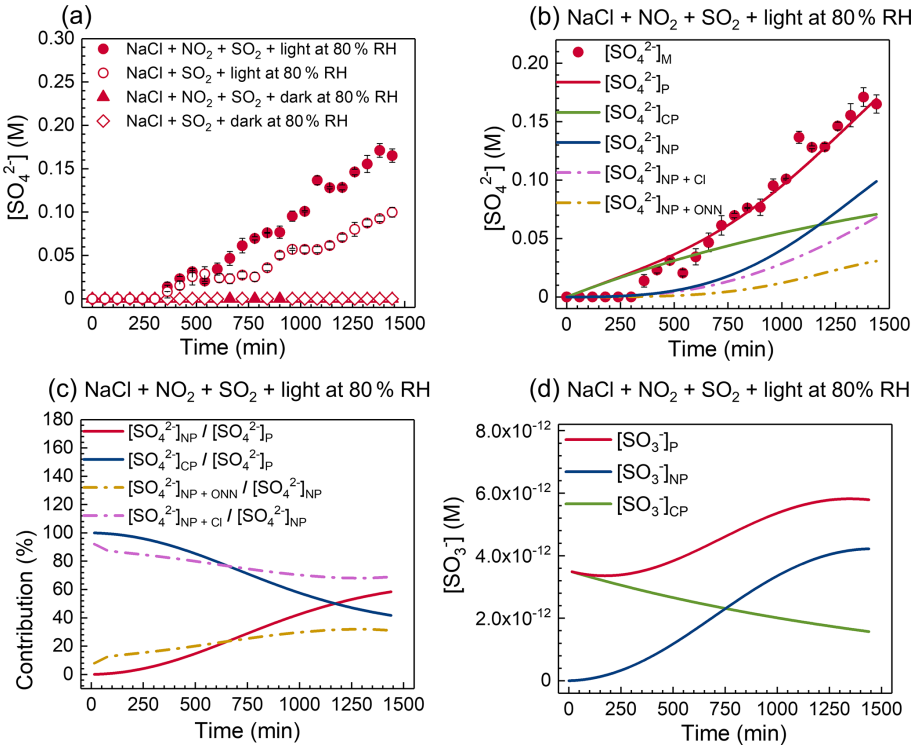

Figure 2. **(a)** Sulfate concentration as a function of time under various conditions, including irradiation/dark experiments and co-uptake/unary uptake experiments at 80 % RH. **(b)** The model-predicted sulfate concentration generated from $[SO_4^{2-}]_{NP}$, $[SO_4^{2-}]_{CP}$, $[SO_4^{2-}]_{NP+Cl}$, and $[SO_4^{2-}]_{NP+ONN}$ pathways. **(c)** The contribution of different formation pathways to sulfate concentration. **(d)** The model-predicted SO_3^- concentration from chloride photolysis and nitrate photolysis. $[SO_4^{2-}]_M$, $[SO_4^{2-}]_P$, and $[SO_3^-]_P$ represent the experimentally measured $[SO_4^{2-}]$, model-predicted $[SO_4^{2-}]$, and model-predicted $[SO_3^-]$, respectively.

$[SO_4^{2-}]_{NP}$ pathway shows an increasing trend, yielding ∼ 58 % of total sulfate after 1440 min (Fig. 2c). We further investigate the role of the $[SO_4^{2-}]_{NP+ONN}$ and $[SO_4^{2-}]_{NP+Cl}$ pathways in the formation of sulfate. As shown in Fig. 2b, the $[SO_4^{2-}]_{NP+ONN}$ and $[SO_4^{2-}]_{NP+Cl}$ pathways contribute to ∼ 18 % and ∼ 40 % of total sulfate production, respectively, after 1440 min. For the $[SO_4^{2-}]_{NP+ONN}$ pathway, the N(III) pathway dominates over the NO_2 pathway and OH pathway in forming sulfate (Fig. S9), which is consistent with our previous works (Gen et al., 2019b, a). The role of the $[SO_4^{2-}]_{NP+ONN}$ pathway relative to the $[SO_4^{2-}]_{NP+Cl}$ pathway becomes important at a later stage. As shown in Fig. 2c, $[SO_4^{2-}]_{NP+ONN} / [SO_4^{2-}]_{NP}$ and $[SO_4^{2-}]_{NP+Cl} / [SO_4^{2-}]_{NP}$ show increasing and decreasing trends, respectively, as the reaction proceeds, which is likely due to the significant chloride depletion near the end (Fig. S4). For the $[SO_4^{2-}]_{NP+Cl}$ pathway, we postulated that OH radicals could promote the formation of reactive chlorine species that can further react with S(IV) to form SO_3^- and then sulfate. Specifically, in the presence of nitrate photolysis and chloride, the OH radicals from nitrate photolysis can react with Cl^- to yield $ClOH^-$ that combines with H^+ to generate $Cl^\bullet$ radicals. The produced $Cl^\bullet$ further reacts with Cl^- to yield $Cl_2^{\bullet-}$, and both can react with HSO_3^- to yield SO_3^-, which undergoes chain reactions to produce sulfate (Table S1). Typically, SO_3^- radicals are mainly produced from the reaction of $OH + HSO_3^-$ or $Cl^\bullet / Cl_2^{\bullet-} + HSO_3^-$ in this study. Figure S10 shows that SO_3^- formed from $OH + HSO_3^-$ is significantly lower than that from $Cl^\bullet / Cl_2^{\bullet-} + HSO_3^-$, further confirming that chlorine chemistry plays a vital role in sulfate formation. Note that $Cl^\bullet / Cl_2^{\bullet-}$ can be generated from chloride photolysis and the NP + Cl process. Figure 2d shows that chloride photolysis only contributes to the significant formation of SO_3^- radicals at the initial stage, and the decreasing trend of SO_3^- indicates that the consumption rate of SO_3^- is higher than the formation rate without the assistance of nitrate photolysis. In contrast, the contribution of nitrate photolysis to SO_3^- concentration increases and dominates over chloride photolysis after ∼ 750 min (Fig. 2d). These results at 80 % RH highlight that interaction between nitrate photolysis and chlorine chemistry is crucial in enhancing sulfate formation.

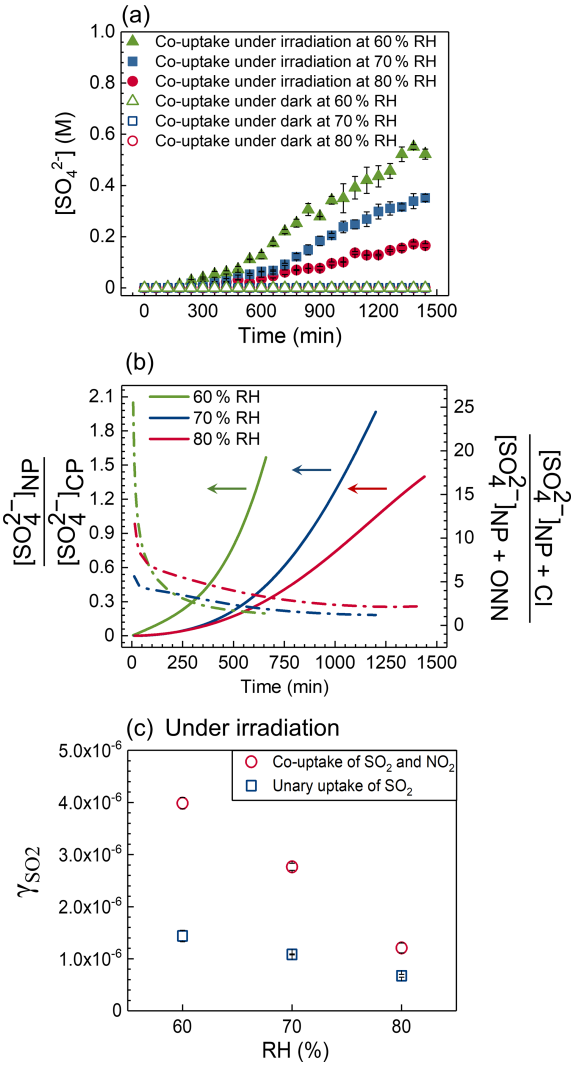

Figure 3. **(a)** Sulfate concentration as a function of time during the co-uptake of NO_2 and SO_2 into NaCl droplets at 60 %, 70 %, and 80 % RH under dark and irradiation conditions. **(b)** $[SO_4^{2-}]_{NP} / [SO_4^{2-}]_{CP}$ and $[SO_4^{2-}]_{NP+Cl} / [SO_4^{2-}]_{NP+ONN}$ as a function of time at 80 %, 70 %, and 60 % RH. The dash-dotted lines in panel **(b)** refer to the right y axis. **(c)** Reactive uptake coefficient of SO_2, γ_{SO_2}, at different RHs under irradiation during co-uptake and unary uptake.

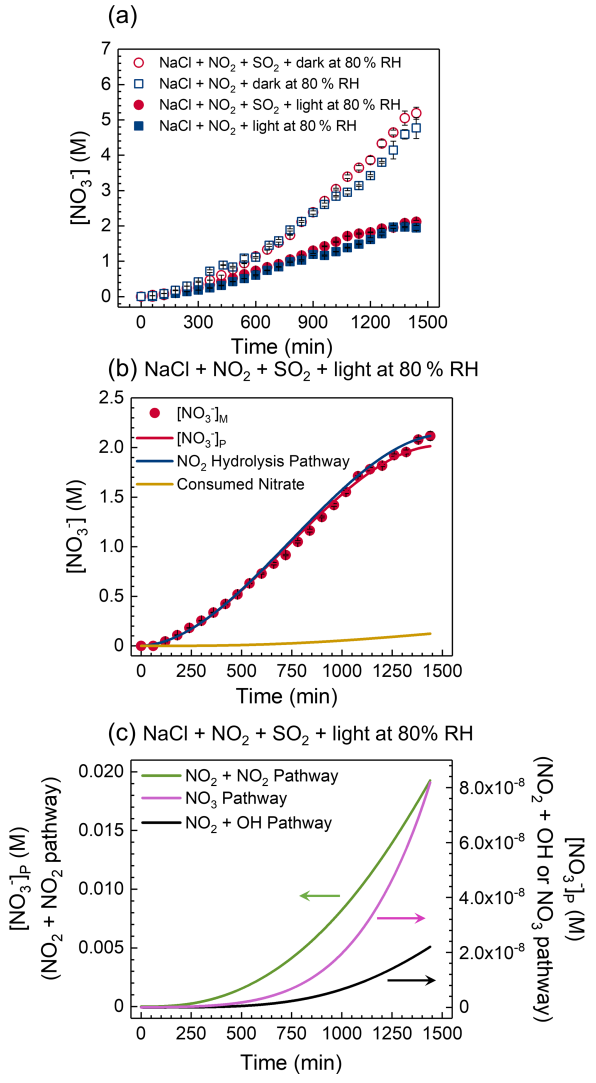

Figure 4. **(a)** The nitrate concentration as a function of time in co-uptake/unary uptake experiments under irradiation/dark conditions at 80 % RH. **(b, c)** The experimentally measured nitrate concentration, $[NO_3^-]_M$, and model-predicted nitrate concentration, $[NO_3^-]_P$, from different pathways during the co-uptake of NO_2 and SO_2 under irradiation at 80 % RH. "Consumed Nitrate" refers to the reduction in nitrate concentration due to nitrate photolysis (i.e., SR1 in Table S1).

3.2 The effect of RH and presence of NO_2 in forming sulfate

As discussed earlier, the direct reaction of NO_2 with S(IV) under dark conditions is not effective in producing sulfate at 80 % RH in this study. Also, no sulfate was observed during the unary uptake of SO_2 into NaCl droplets under dark conditions (Fig. 2a). The same was found at 60 % and 70 % RH (Fig. 3a). Therefore, we focused on the RH dependence of sulfate production rates in the presence of irradiation. Note that 60 % RH is below the deliquescence point of NaCl particles and the particles existed as supersaturated droplets.

As shown in Figs. 3a and S11, the sulfate production rate (with units of $M\,s^{-1}$), $d[SO_4^{2-}]/dt$, increases with decreasing RH, which is attributed to the increased concentrations of oxidants (i.e., OH radical, NO_2, N(III), and $Cl^{\bullet} / Cl_2^{\bullet-}$) at low RH, irrespective of the presence of NO_2 or not. It should be noted that the total sulfate production rate (with units of $mol\,s^{-1}$), $d(n(SO_4^{2-}))/dt$, depends on the size of the droplets. However, the comparable droplet size utilized in all experiments implies $d(n(SO_4^{2-}))/dt$ follows the same trends as $d[SO_4^{2-}]/dt$. For unary SO_2 uptake experiments, the sulfate production rate increases from 1.3×10^{-6} to

$3.3 \times 10^{-6}\,M\,s^{-1}$ when RH decreases from 80 % to 60 % RH (Table S4). During the co-uptake course of NO_2 and SO_2, sulfate concentrations tend to follow a sigmoidal trend with a slow initial increase followed by a rapid one before slowing down, especially at low RH (Fig. 3a). Table S4 shows the averaged sulfate production rates of the initial and the fast-growing stages. The sulfate production rate at the initial stage is comparable to that observed during the unary uptake of SO_2 by NaCl particles under irradiation at all RHs (Fig. S12 and Table S4), indicating chloride photolysis plays a major role in forming sulfate, where nitrate concentration is less than 1 M (Fig. 4a). Such low nitrate concentration cannot significantly affect sulfate production. Enhanced sulfate production was observed at the second stage when nitrate concentration reached up to a few molar. This enhancement resulted from the nitrate photolysis and its interaction with chlorine chemistry, as discussed earlier. The sulfate production rate at the second stage increases from 2.7×10^{-6} to $8.6 \times 10^{-6}\,M\,s^{-1}$ as RH decreases from 80 % to 60 % RH (Table S4). The slower sulfate production rate near the end is likely due to significant chloride consumption resulting from photolysis and evaporation. Figures 2b and S13 show the predicted sulfate concentration from $[SO_4^{2-}]_{CP}$, $[SO_4^{2-}]_{NP}$, $[SO_4^{2-}]_{NP+Cl}$, and $[SO_4^{2-}]_{NP+ONN}$ pathways at 80 %, 70 %, and 60 % RH. The model simulation times are ∼ 660 min, ∼ 1200 min, and ∼ 1440 min for 60 %, 70 %, and 80 % RH, respectively (Figs. 2b and S13), after which nitrate concentrations have increased beyond the range of the calibration shown in Fig. S2. $[SO_4^{2-}]_{CP}$ contributes a large fraction (> 95 %) of total sulfate production before 250 min at all RHs (Figs. 2c and S13), consistent with observations from experiments (Fig. S12) and further confirming that chloride photolysis plays a dominant role in sulfate formation in the early stage. The role of $[SO_4^{2-}]_{NP}$ appears to be more important at a later stage (Figs. 2c and S13), especially at low RH because of the higher nitrate concentration. As shown in Fig. 3b, $[SO_4^{2-}]_{NP} / [SO_4^{2-}]_{CP}$ increases faster at low RH. In addition, a $[SO_4^{2-}]_{NP+Cl}$-to-$[SO_4^{2-}]_{NP+ONN}$ ratio significantly larger than unity was found in all studied RHs, suggesting the combined effect of nitrate photolysis and chlorine chemistry exerts a crucial impact on enhanced sulfate formation (Fig. 3b).

Furthermore, the reactive uptake coefficients of SO_2, γ_{SO_2}, were compared for unary uptake and co-uptake to investigate the impact of NO_2 in sulfate formation. We focused on the irradiation results because there was no evident sulfate production under dark conditions irrespective of NO_2 presence or not (Fig. 2a). It should be noted the γ_{SO_2} of co-uptake shown in Fig. 3c is derived from the fast-growing (second) stage of sulfate formation (Fig. S12), the regime where the combined effect of nitrate photolysis and chlorine chemistry plays a crucial role. The γ_{SO_2} increases with decreasing RH, with larger impacts in the presence of NO_2 (Fig. 3c and Table S5). In the absence of NO_2, enhanced γ_{SO_2} mainly results from the increased reactive chlorine species produced from chloride photolysis at high concentrations of chloride at low RH. The presence of NO_2 significantly increased γ_{SO_2} (Fig. 3c) further due to nitrate photolysis. The γ_{SO_2} of co-uptake increased by a factor of ∼ 1.7, ∼ 2.5, and ∼ 2.9 at 80 %, 70 %, and 60 % RH, respectively, compared to that of unary uptake. These results imply that the effect of NO_2 in forming sulfate becomes more important at low RH. To highlight the importance of the effect of nitrate photolysis and chloride photolysis in forming sulfate due to the presence of NO_2, we developed an equation of γ_{SO_2} as a function of the nitrate photolysis rate, $P_{NO_3^-}$ ($j_{NO_3^-} \times [NO_3^-]$), and chloride photolysis rate, P_{Cl^-} ($j_{Cl^-} \times [Cl^-]$), as $\gamma_{SO_2} = 0.41 \times P_{NO_3^-} + 0.34 \times P_{Cl^-}$, based on the experimental results from the co-uptake of NO_2 and SO_2 under irradiation at three RHs. The derived expression matched with the experimental data points well (Fig. S14). Our experimental results pertain to $[NO_3^-] / [Cl^-]$ below 3, and the derived equation applies to the system involving both nitrate and chloride . Extrapolation beyond this range should be done with caution.

3.3 Mechanisms of nitrate formation during the uptake

As discussed, there was significant nitrate formation under both dark and irradiation conditions. Under dark conditions, it is mainly produced from NO_2 hydrolysis regardless of the presence of SO_2 or not, hereafter referred to as the "NO_2 hydrolysis pathway". Previous studies reported the reaction of NO_2 with Cl^- ($2NO_2(aq) + Cl^-(aq) \rightarrow NO_3^-(aq) + ClNO(g)$), which can also yield nitrate (Karlsson and Ljungström, 1998; Weis and Ewing, 1999). To investigate whether this process is also responsible for the significant formation of nitrate under dark conditions, we performed a control experiment with unary uptake of NO_2 into $(NH_4)_2SO_4$ droplets at 80 % RH. As shown in Fig. S15, prompt nitrate formation was also observed in $(NH_4)_2SO_4$ droplets at a rate just slightly lower than NaCl droplets. This result indicates that the role of the reaction of NO_2 with chloride in forming nitrate is minor, but NO_2 hydrolysis plays a dominant role in the formation of nitrate under dark conditions. During the co-uptake, the available S(IV) without being oxidized under dark conditions can further promote NO_2 uptake and nitrate formation (Fig. 5b), as will be discussed later. Under irradiation, NO_2 from reactive uptake can also react with OH radicals or NO_2 from nitrate photolysis can form nitrate, denoted as "$NO_2 + OH$ pathway" and "$NO_2 + NO_2$ pathway", respectively. Besides, NO_3 radicals can undergo radical chain reactions to produce nitrate (Table S1), referred to as the "NO_3 pathway".

Figure 4a shows the nitrate concentration trends of co-uptake/unary uptake of NO_2 under irradiation/dark conditions at 80 % RH. A significant amount of nitrate was observed via the reactive uptake of NO_2 into NaCl

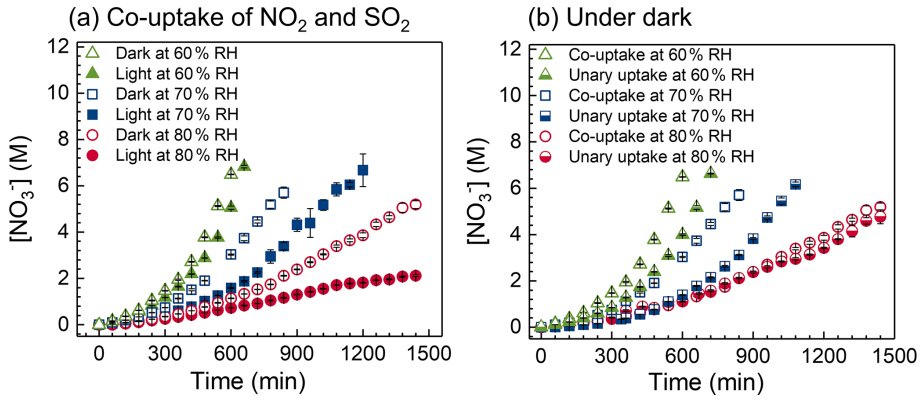

Figure 5. **(a)** Nitrate concentration as a function of time during the co-uptake of NO_2 and SO_2 into NaCl droplets at different RHs under dark and irradiation conditions. **(b)** Nitrate concentration as a function of time under various conditions, including co-uptake of NO_2 and SO_2 and unary uptake of NO_2 under dark conditions at 60 %, 70 %, and 80 % RH.

droplets. The presence of SO_2 has little effect on NO_2 uptake at 80 % RH. Under dark conditions, an exponential increase in nitrate production was observed, particularly at low RH (Figs. 4a and 5a). The pH in these dark experiments decreased during the uptake (Fig. S5). However, it is known that increased acidity (i.e., decreased pH) due to hydrolysis is not conducive to NO_2 uptake (Seinfeld and Pandis, 2006). We speculated that chloride depletion plays a mechanistic role in the exponential increase in nitrate concentration. NO_2 uptake converts NaCl to $NaNO_3$, which lowers the hygroscopicity of the droplet (Clegg et al., 1997). resulting in a droplet shrinkage of $\sim$ 10 % after 1440 min uptake (Fig. S16). We used E-AIM to estimate chloride and nitrate concentrations at different molar ratios of chloride to nitrate, $[Cl^-]/[NO_3^-]$, at a given RH. As shown in Fig. S17, nitrate concentration increased exponentially when $[Cl^-]/[NO_3^-]$ decreased below 3 due to the lower hygroscopicity of $NaNO_3$ compared to NaCl, i.e., decreasing liquid water content of the droplet, which may partially explain the observed exponential increase in nitrate concentration in Figs. 4a and 5a. The overall trend is that the nitrate production rate is higher under dark than under irradiation conditions, which may be partly due to nitrate photolysis at 80 % RH.

Furthermore, we examined the time series of nitrate concentration during the co-uptake at 80 % RH under irradiation to elucidate the nitrate formation mechanism using the kinetic model. Figure 4b and c show the contributions of different pathways to nitrate during the co-uptake of NO_2 and SO_2 under irradiation. The NO_2 hydrolysis pathway yields $\sim$ 2.1 M nitrate, but the $NO_2 + NO_2$ pathway, $NO_2 + OH$ pathway, and NO_3 pathway altogether contribute to only $\sim$ 0.02 M nitrate after 1440 min. Hence, NO_2 hydrolysis is dominant in nitrate formation. The presence of chloride and S(IV) can consume the oxidants (e.g., OH radicals and chlorine species), potentially making those three pathways ineffective in forming nitrate (Table S1). Among these three pathways, the $NO_2 + NO_2$ pathway (left axis, Fig. 4c) contributes most to nitrate, and the other two pathways are negligible (right axis). Note that $\sim$ 0.1 M nitrate was consumed due to nitrate photolysis (i.e., SR1 in Table S1) after 1440 min. This minor consumption of nitrate due to photolysis is related to the low nitrate photolysis rate constant ($\sim 1.4 \times 10^{-6}$ s^{-1} at 80 % RH), based on fitting the experimental results, which is about 1 order of magnitude lower than that fitted in our previous works (Gen et al., 2019b; Zhang et al., 2020, 2021). The photolysis rate constant is typically proportional to the light intensity. Also, it is known that nitrate has a maximum absorption band at $\sim$ 302 nm (Gen et al., 2022). The light intensity at 300 nm of the xenon lamp used in the current study is around 3 orders of magnitude lower than that of the single-line 300 nm lamp used in our earlier works (Gen et al., 2020).

In the unary uptake of NO_2 into NaCl droplets under irradiation, NO_2 hydrolysis still dominates over those three pathways initiated by nitrate photolysis (Fig. S18). However, in addition to the $NO_2 + NO_2$ pathway, the NO_3 pathway also makes a non-negligible contribution to nitrate formation during the unary uptake of NO_2 compared to that during the co-uptake. The reaction of $Cl_2^{\bullet-}$ with NO_3 (SR50 in Table S1) is a dominant process of the NO_3 pathway. However, in the co-uptake experiments, the consumption of $Cl_2^{\bullet-}$ by S(IV) (SR59 in Table S1) makes nitrate production by the reaction of chlorine species with NO_3 radicals ineffective (Fig. S19).

3.4 The effect of RH and presence of SO_2 in forming nitrate

We further investigate the effect of RH on the nitrate production rate during the uptake. In all experiments, including unary uptake/co-uptake under dark/irradiation conditions, the nitrate production rate increased with decreasing RH (Figs. 5 and S20), which is attributed to the increased NaCl concentration at low RH. A prior study

reported an enhanced uptake coefficient of NO_2 at increasing concentration of NaCl solutions (Yabushita et al., 2009). Figure 5a shows the nitrate formation during the co-uptake under both dark and irradiation conditions at different RHs. The nitrate concentration increased slowly initially, with a faster increase at a later stage at all RHs, attributable to chloride depletion, as discussed earlier. Under dark conditions, NO_2 hydrolysis and the reaction of NO_2 with S(IV) are the only two reactions occurring in droplets, with the former being the sole pathway in forming nitrate. Under irradiation, similarly to the 80 % RH experiments, the NO_2 hydrolysis pathway dominated the contribution to nitrate at 60 % and 70 % RH (Fig. S21). The nitrate concentration under irradiation during the co-uptake was lower than those concentrations under dark conditions at all RHs. However, the difference between dark and irradiation conditions became smaller with decreasing RH. We speculate that the faster nitrate production at low RH can compensate for the consumption of nitrate due to photolysis. Such phenomena were also observed during the unary uptake under dark and irradiation conditions (Fig. S20a).

We also investigated the effect of SO_2 on nitrate production under dark and irradiation conditions. Figure 5b shows that the presence of SO_2 promotes nitrate formation under dark conditions, especially at low RH. We proposed that such enhancement might be closely associated with the reaction between NO_2 and HSO_3^-. The increase in HSO_3^- peak intensity during unary uptake of SO_2 into NaCl under dark conditions indicates the formation of HSO_3^- from SO_2 dissolution is feasible in our system (Fig. S22). The formed HSO_3^- from reactive uptake of SO_2 into particles prefers to stay at the surface of an aerosol particle (Yang et al., 2019), and in turn, it may pull more NO_2 into droplets during the co-uptake due to the interaction between NO_2 and HSO_3^- (Tang and Li, 2021). The higher formation rate of HSO_3^- at low RH during unary SO_2 uptake into NaCl may explain the more considerable difference in nitrate concentration between co-uptake and unary uptake at low RH than at 80 % RH (Fig. 5b). In contrast, nitrate concentrations between co-uptake and unary uptake under irradiation are comparable (Fig. S20b). We proposed that HSO_3^- may undergo photooxidation rapidly to convert into sulfate; hence its role in pulling more NO_2 into droplets becomes limited under irradiation during the co-uptake. These findings open up new perspectives on the enhanced formation of nitrate with the involvement of SO_2, especially at low RH.

4 Atmospheric implications

Built on the well-known process of SO_2 oxidation by NO_2 in forming sulfate under dark conditions, we examined sulfate formation during the co-uptake of SO_2 and NO_2 in NaCl droplets under irradiation in this work. In our earlier works, we examined the effect of nitrate photolysis in forming sulfate and glyoxal-derived secondary organic aerosol (SOA; Zhang et al., 2020, 2021, 2022; Gen et al., 2019a, b). The present study indicates a previously unrecognized role of the combined effect of nitrate photolysis and chlorine chemistry in enhanced sulfate formation, which is expected to have important implications for atmospheric chemistry. In brief, the OH radicals formed from nitrate photolysis can react with chloride ions to promote the formation of chlorine species (e.g., $Cl^{\bullet}$ and $Cl_2^{\bullet-}$) and further enhance sulfate formation. Such an effect enhances the γ_{SO_2} by factors of ~ 1.7, ~ 2.5, and ~ 2.9 at 80 %, 70 %, and 60 % RH, respectively, at $0.2 < [NO_3^-]/[Cl^-] < 3$, compared to those from the chloride photolysis (i.e., $NaCl + SO_2 +$ light conditions).

To further verify whether our proposed mechanism could apply to urban sites, where ammonium salts are the major components of particles, we performed additional experiments with SO_2 uptake into premixed $NH_4Cl + NH_4NO_3$ (4 : 1 mole ratio) droplets and pure NH_4Cl droplets under the same irradiation at 75 % RH. Figure S23a shows a higher sulfate production rate in pure NH_4NO_3 droplets, likely due to the higher initial nitrate concentration in pure NH_4NO_3 droplets (~ 8.1 M) than in premixed $NH_4Cl + NH_4NO_3$ droplets (~ 1.0 M). As reported in our earlier works, nitrate photolysis could also promote sulfate formation. Hence, sulfate concentration is normalized by initial nitrate concentration, as shown in Fig. S23b. A significant enhancement in the normalized sulfate production rate was observed in premixed $NH_4Cl + NH_4NO_3$ droplets, confirming that the interplay of nitrate photolysis and chlorine chemistry could also be taking place. Note that the uptake coefficient equation ($\gamma_{SO_2} = 0.41 \times P_{NO_3^-} + 0.34 \times P_{Cl^-}$) is based on the experimental results of the co-uptake of NO_2 and SO_2 into NaCl droplets under irradiation at 60 %, 70 %, and 80 % RH. To evaluate if this equation is applicable to non-sea-salt systems, we compared γ_{SO_2} from the equation with that from the experimental result (i.e., premixed $NH_4Cl + NH_4NO_3$ system) in Fig. S23a. The calculated γ_{SO_2} (2.6×10^{-6}) agrees well with that from the experiment (3.0×10^{-6}) (Text S2). This gives us confidence that the derived expression of the uptake coefficient may be useful in ammonium systems containing nitrate and chloride too. In our earlier work, we performed unary uptake of SO_2 into premixed $NH_4Cl + NH_4NO_3$ droplets under 300 nm irradiation at different $[NO_3^-]/[Cl^-]$ ratios, in air and N_2 environments (Zhang et al., 2020). Note that the presence of O_2 (air environment) is essential for sulfate formation from reactions of reactive chlorine species with HSO_3^- (Fig. 1). The normalized sulfate production rate continuously increases as $[NO_3^-]/[Cl^-]$ decreases in air, but no further enhancement of the sulfate production rate was observed in N_2 when $[NO_3^-]/[Cl^-] < 5$ (Zhang et al., 2020). Such

results also support the assertion that the combined effect of nitrate photolysis and chlorine chemistry in promoting sulfate formation may be applicable in ammonium systems containing nitrate and chloride. These results highlighted that the co-existence of nitrate photolysis and chlorine chemistry can increase the atmospheric oxidative capacity and enhance the formation of sulfate. Further investigations into the combined effect of nitrate photolysis and chlorine chemistry in forming SOA are proposed.

Prior studies have pointed out that chlorine atoms ($Cl^{\bullet}$) can play an essential role in increasing atmospheric capacity and the formation of secondary pollutants and ozone (Qiu et al., 2019a; Li et al., 2021; Liao et al., 2014). Typically, $Cl^{\bullet}$ can form from the photo-dissociation and oxidation of inorganic chlorine species (e.g., Cl_2 and $ClNO_2$) and chlorinated organic species (e.g., $CHCl_3$ and CH_2Cl_2) (Priestley et al., 2018; Y. Wang et al., 2020). $Cl^{\bullet}$ is much more reactive than OH radicals (Su et al., 2022; Hossaini et al., 2016), although it typically has lower concentrations and is in limited regions of the atmosphere compared to the OH radicals (Wang and Hildebrandt Ruiz, 2018; Saiz-Lopez and Von Glasow, 2012). Laboratory studies have shown the importance of $Cl^{\bullet}$ for the oxidation of volatile organic compound (VOC) precursors (e.g., common monoterpenes, isoprene, toluene, and alkanes) in forming SOA (Masoud and Ruiz, 2021; Dhulipala et al., 2019; Wang and Ruiz, 2017; Riva et al., 2015). The rate constant of $Cl^{\bullet}$ with most atmospherically relevant VOCs is up to 2 orders of magnitude higher than the rate constant of OH-initiated oxidation (Masoud and Ruiz, 2021). In addition to nitrate and sulfate formation, the current study provides new insight into the enhanced formation of chlorine species due to nitrate photolysis. Recently, Peng et al. (2022) proposed that nitrate photolysis at high aerosol acidity is an important pathway for activating inert chloride to produce photolabile Cl_2, which is a highly reactive species and can strongly affect the abundance of climate- and air-quality-relevant trace gases, during the daytime in the polluted period. As suggested with the reactions in this study, Peng et al. (2022) also suggested that OH radicals produced from nitrate photolysis can further oxidize chloride ions to enhance the formation of Cl_2. Our kinetic model also indicates that $Cl^{\bullet}$ generated from chloride photolysis could also undergo self-reaction to form Cl_2. However, no Cl_2 production was observed in Peng et al. (2022) when illuminating NaCl solution, likely due to ineffective photolysis in bulk solution compared to the droplet. Note that $Cl^{\bullet}$ can also react with S(IV) in the presence of SO_2, competing with the bimolecular reaction of $Cl^{\bullet}$. We used the kinetic model to simulate the effect of SO_2 uptake in forming Cl_2. As shown in Fig. S24, the simulated Cl_2 concentration is 3–4 orders of magnitude lower in the presence of SO_2 than in its absence, suggesting that the presence of SO_2 may inhibit the formation of Cl_2. However, Peng et al. (2022) suggested that reducing SO_2 concentration would slow the Cl_2 production due to the reduced particle acidity. Hence, further systematic studies on such effects are needed in the future.

Recent studies have emphasized the increased contribution of nitrate to $PM_{2.5}$ pollution (Fu et al., 2020; Itahashi et al., 2018; H. Li et al., 2019). Thus, identifying the key factors contributing to particulate nitrate formation and driving its trend is critical to eliminating winter haze episodes. The heterogeneous uptake of NO_2 onto aqueous particles, mineral dust, and urban grime with subsequent hydrolysis to form nitrate and HONO has been reported (Liu et al., 2019; Pandit et al., 2021; Xu et al., 2019; Li et al., 2018b; Yu et al., 2021; Dyson et al., 2021; Martins-Costa et al., 2020; Tan et al., 2016). The γ_{NO_2} is a crucial parameter controlling the heterogeneous chemistry on the aerosol surface in the chemical transport model (McDuffie et al., 2018; Xie et al., 2022). We used the experimentally measured nitrate formation rate from unary uptake of NO_2 into NaCl droplets under dark conditions at all RHs to estimate the γ_{NO_2} in NaCl droplets in this study. The averaged γ_{NO_2} values are 1.6×10^{-5}, 1.9×10^{-5}, and 3.0×10^{-5} at 80 %, 70 %, and 60 % RH, respectively. Higher γ_{NO_2} was observed at low RH, where NaCl droplets achieve supersaturation. Previous studies have also reported a much higher uptake coefficient of NO_2 of $\sim 10^{-4}$ on NaCl particles compared to other inorganic particles (e.g., $(NH_4)_2SO_4$) (Abbatt and Waschewsky, 1998; Harrison and Collins, 1998; Tan et al., 2016; Ge et al., 2019), whose uptakes coefficient range from $< 10^{-8}$ to 10^{-7} (Yu et al., 2021). However, Yu et al. (2021) reported a much smaller γ_{NO_2} on NaCl with the value of $\sim 10^{-8}$ (Yu et al., 2021). Existing studies report a wide range of γ_{NO_2} values (M. Li et al., 2019; Miao et al., 2020), making it difficult for modelers to estimate the contribution of the heterogeneous uptake of NO_2 and hydrolysis to forming nitrate. For instance, it has been reported that the mean contribution of NO_2 hydrolysis to particulate nitrate formation is 6.3 %–19 %, which increases to 35.9 % during extreme-haze days (Xie et al., 2022; Qiu et al., 2019b; Chan et al., 2021).

In addition, our results also highlighted that the presence of SO_2 can effectively promote the formation of nitrate further, especially during the nighttime. In other words, controlling SO_2 emissions not only reduces sulfate formation, but also slows nitrate formation. Therefore, systematic investigations of the factors, including ionic strength, seed particle types (e.g., nitrate- and sulfate-containing particles), and other gas species, that impact NO_2 uptake and nitrate formation are needed in the future to further constrain the contribution of NO_2 hydrolysis to nitrate formation more accurately.

Data availability. The data are available upon request to the corresponding authors.

Supplement. The supplement related to this article is available online at: https://doi.org/10.5194/acp-23-6113-2023-supplement.

Author contributions. RZ and CKC designed the whole research. RZ conducted experiments and kinetic model simulation. RZ and CKC analyzed the experimental data and wrote the paper.

Competing interests. The contact author has declared that neither of the authors has any competing interests.

Disclaimer. Publisher's note: Copernicus Publications remains neutral with regard to jurisdictional claims in published maps and institutional affiliations.

Acknowledgements. This work was supported by the National Natural Science Foundation of China (nos. 42075100 and 42275104), the Guangdong Basic and Applied Basic Research Foundation (2020B1515130003), and the Hong Kong Research Grants Council (11304121).

Financial support. This research has been supported by the Guangdong Basic and Applied Basic Research Foundation (grant no. 2020B1515130003), Hong Kong Research Grants Council (grant nos. 11304121 and 11314222), and National Natural Science Foundation of China (grant nos. 42075100 and 42275104).

Review statement. This paper was edited by Manabu Shiraiwa and reviewed by two anonymous referees.

References

Abbatt, J. and Waschewsky, G.: Heterogeneous interactions of HOBr, HNO_3, O_3, and NO_2 with deliquescent NaCl aerosols at room temperature, J. Phys. Chem. A, 102, 3719–3725, 1998.

Alexander, B., Hastings, M. G., Allman, D. J., Dachs, J., Thornton, J. A., and Kunasek, S. A.: Quantifying atmospheric nitrate formation pathways based on a global model of the oxygen isotopic composition ($\Delta^{17}O$) of atmospheric nitrate, Atmos. Chem. Phys., 9, 5043–5056, https://doi.org/10.5194/acp-9-5043-2009, 2009.

Arakaki, T., Miyake, T., Hirakawa, T., and Sakugawa, H.: pH Dependent Photoformation of Hydroxyl Radical and Absorbance of Aqueous-Phase N(III) (HNO_2 and NO_2^-), Environ. Sci. Technol., 33, 2561–2565, https://doi.org/10.1021/es980762i, 1999.

Chan, C. K. and Yao, X.: Air pollution in mega cities in China, Atmos. Environ., 42, 1–42, https://doi.org/10.1016/j.atmosenv.2007.09.003, 2008.

Chan, Y. C., Evans, M. J., He, P., Holmes, C. D., Jaeglé, L., Kasibhatla, P., Liu, X. Y., Sherwen, T., Thornton, J. A., and Wang, X.: Heterogeneous nitrate production mechanisms in intense haze events in the North China Plain, J. Geophys. Res.-Atmos., 126, e2021JD034688, https://doi.org/10.1029/2021JD034688, 2021.

Cheng, Y., Zheng, G., Wei, C., Mu, Q., Zheng, B., Wang, Z., Gao, M., Zhang, Q., He, K., and Carmichael, G.: Reactive nitrogen chemistry in aerosol water as a source of sulfate during haze events in China, Sci. Adv., 2, e1601530, https://doi.org/10.1126/sciadv.1601530, 2016.

Clegg, S. L., Brimblecombe, P., Liang, Z., and Chan, C. K.: Thermodynamic Properties of Aqueous Aerosols to High Supersaturation: II – A Model of the System Na^+-Cl^--NO_3^--SO_4^{2-}-H_2O at 298.15 K, Aerosol Sci. Technol., 27, 345–366, 1997.

Clegg, S. L., Brimblecombe, P., and Wexler, A. S.: Thermodynamic model of the system H^+-NH_4^+-Na^+-SO_4^{2-}-NO_3^--Cl^--H_2O at 298.15 K, J. Phys. Chem. A, 102, 2155–2171, 1998.

Corbett, J. J., Winebrake, J. J., Green, E. H., Kasibhatla, P., Eyring, V., and Lauer, A.: Mortality from ship emissions: a global assessment, Environ. Sci. Technol., 41, 8512–8518, 2007.

Craig, R. L., Peterson, P. K., Nandy, L., Lei, Z., Hossain, M. A., Camarena, S., Dodson, R. A., Cook, R. D., Dutcher, C. S., and Ault, A. P.: Direct determination of aerosol pH: Size-resolved measurements of submicrometer and supermicrometer aqueous particles, Anal. Chem., 90, 11232–11239, 2018.

Dhulipala, S. V., Bhandari, S., and Ruiz, L. H.: Formation of oxidized organic compounds from Cl-initiated oxidation of toluene, Atmos. Environ., 199, 265–273, 2019.

Dyson, J. E., Boustead, G. A., Fleming, L. T., Blitz, M., Stone, D., Arnold, S. R., Whalley, L. K., and Heard, D. E.: Production of HONO from NO_2 uptake on illuminated TiO_2 aerosol particles and following the illumination of mixed TiO_2 / ammonium nitrate particles, Atmos. Chem. Phys., 21, 5755–5775, https://doi.org/10.5194/acp-21-5755-2021, 2021.

Fu, X., Wang, T., Gao, J., Wang, P., Liu, Y., Wang, S., Zhao, B., and Xue, L.: Persistent Heavy Winter Nitrate Pollution Driven by Increased Photochemical Oxidants in Northern China, Environ. Sci. Technol., 54, 3881–3889, https://doi.org/10.1021/acs.est.9b07248, 2020.

Gardner, E. P., Sperry, P. D., and Calvert, J. G.: Primary quantum yields of NO_2 photodissociation, J. Geophys. Res.-Atmos., 92, 6642–6652, 1987.

Ge, S., Wang, G., Zhang, S., Li, D., Xie, Y., Wu, C., Yuan, Q., Chen, J., and Zhang, H.: Abundant NH_3 in China Enhances Atmospheric HONO Production by Promoting the Heterogeneous Reaction of SO_2 with NO_2, Environ. Sci. Technol., 53, 14339–14347, https://doi.org/10.1021/acs.est.9b04196, 2019.

Gen, M., Zhang, R., Huang, D. D., Li, Y., and Chan, C. K.: Heterogeneous Oxidation of SO_2 in Sulfate Production during Nitrate Photolysis at 300 nm: Effect of pH, Relative Humidity, Irradiation Intensity, and the Presence of Organic Compounds, Environ. Sci. Technol., 53, 8757–8766, https://doi.org/10.1021/acs.est.9b01623, 2019a.

Gen, M., Zhang, R., Huang, D. D., Li, Y., and Chan, C. K.: Heterogeneous SO_2 Oxidation in Sulfate Formation by Photolysis of Particulate Nitrate, Environ. Sci. Technol. Lett., 6, 86–91, https://doi.org/10.1021/acs.estlett.8b00681, 2019b.

Gen, M., Zhang, R., Li, Y., and Chan, C. K.: Multiphase Photochemistry of Iron-Chloride Containing Particles as a Source of Aqueous Chlorine Radicals and Its Effect on Sulfate Production, Environ. Sci. Technol., 54, 9862–9871, https://doi.org/10.1021/acs.est.0c01540, 2020.

Gen, M., Zhang, R., and Chan, C. K.: Nitrite/Nitrous Acid Generation from the Reaction of Nitrate and Fe (II) Promoted by Photolysis of Iron–Organic Complexes, Environ. Sci. Technol., 55, 15715–15723, 2021.

Gen, M., Liang, Z., Zhang, R., Mabato, B. R. G., and Chan, C. K.: Particulate nitrate photolysis in the atmosphere, Environ. Sci.: Atmos., 2, 111–127, https://doi.org/10.1039/D1EA00087J, 2022.

Grossweiner, L. and Matheson, M.: The kinetics of the dihalide ions from the flash photolysis of aqueous alkali halide solutions, J. Phys. Chem., 61, 1089–1095, 1957.

Harrison, R. M. and Collins, G. M.: Measurements of reaction coefficients of NO_2 and HONO on aerosol particles, J. Atmos. Chem., 30, 397–406, 1998.

Hossaini, R., Chipperfield, M. P., Saiz-Lopez, A., Fernandez, R., Monks, S., Feng, W., Brauer, P., and Von Glasow, R.: A global model of tropospheric chlorine chemistry: Organic versus inorganic sources and impact on methane oxidation, J. Geophys. Res.-Atmos., 121, 14271–14297, 2016.

Itahashi, S., Yumimoto, K., Uno, I., Hayami, H., Fujita, S.-I., Pan, Y., and Wang, Y.: A 15-year record (2001–2015) of the ratio of nitrate to non-sea-salt sulfate in precipitation over East Asia, Atmos. Chem. Phys., 18, 2835–2852, https://doi.org/10.5194/acp-18-2835-2018, 2018.

Kalmár, J., Dóka, É., Lente, G., and Fábián, I.: Aqueous photochemical reactions of chloride, bromide, and iodide ions in a diode-array spectrophotometer. Autoinhibition in the photolysis of iodide ions, Dalton T., 43, 4862–4870, 2014.

Karlsson, R. and Ljungström, E.: A Laboratory Study of the Interaction of NH_3 and NO_2 with Sea Salt Particles, Water Air Soil Pollut., 103, 55–70, https://doi.org/10.1023/A:1004972228592, 1998.

Laskin, A., Moffet, R. C., Gilles, M. K., Fast, J. D., Zaveri, R. A., Wang, B., Nigge, P., and Shutthanandan, J.: Tropospheric chemistry of internally mixed sea salt and organic particles: Surprising reactivity of NaCl with weak organic acids, J. Geophys. Res.-Atmos., 117, D15302, https://doi.org/10.1029/2012JD017743, 2012.

Li, H., Cheng, J., Zhang, Q., Zheng, B., Zhang, Y., Zheng, G., and He, K.: Rapid transition in winter aerosol composition in Beijing from 2014 to 2017: response to clean air actions, Atmos. Chem. Phys., 19, 11485–11499, https://doi.org/10.5194/acp-19-11485-2019, 2019.

Li, J., Zhang, N., Wang, P., Choi, M., Ying, Q., Guo, S., Lu, K., Qiu, X., Wang, S., and Hu, M.: Impacts of chlorine chemistry and anthropogenic emissions on secondary pollutants in the Yangtze river delta region, Environ. Pollut., 287, 117624, https://doi.org/10.1016/j.envpol.2021.117624, 2021.

Li, L., Hoffmann, M. R., and Colussi, A. J.: Role of Nitrogen Dioxide in the Production of Sulfate during Chinese Haze-Aerosol Episodes, Environ. Sci. Technol., 52, 2686–2693, https://doi.org/10.1021/acs.est.7b05222, 2018a.

Li, L., Duan, Z., Li, H., Zhu, C., Henkelman, G., Francisco, J. S., and Zeng, X. C.: Formation of HONO from the NH_3-promoted hydrolysis of NO_2 dimers in the atmosphere, P. Natl. Acad. Sci. USA, 115, 7236–7241, 2018b.

Li, M., Su, H., Li, G., Ma, N., Pöschl, U., and Cheng, Y.: Relative importance of gas uptake on aerosol and ground surfaces characterized by equivalent uptake coefficients, Atmos. Chem. Phys., 19, 10981–11011, https://doi.org/10.5194/acp-19-10981-2019, 2019.

Liao, J., Huey, L. G., Liu, Z., Tanner, D. J., Cantrell, C. A., Orlando, J. J., Flocke, F. M., Shepson, P. B., Weinheimer, A. J., Hall, S. R., Ullmann, K., Beine, H. J., Wang, Y., Ingall, E. D., Stephens, C. R., Hornbrook, R. S., Apel, E. C., Riemer, D., Fried, A., Mauldin, R. L., Smith, J. N., Staebler, R. M., Neuman, J. A., and Nowak, J. B.: High levels of molecular chlorine in the Arctic atmosphere, Nat. Geosci., 7, 91–94, https://doi.org/10.1038/ngeo2046, 2014.

Lin, Y.-C., Zhang, Y.-L., Fan, M.-Y., and Bao, M.: Heterogeneous formation of particulate nitrate under ammonium-rich regimes during the high-$PM_{2.5}$ events in Nanjing, China, Atmos. Chem. Phys., 20, 3999–4011, https://doi.org/10.5194/acp-20-3999-2020, 2020.

Liu, J., Li, S., Mekic, M., Jiang, H., Zhou, W., Loisel, G., Song, W., Wang, X., and Gligorovski, S.: Photoenhanced Uptake of NO_2 and HONO Formation on Real Urban Grime, Environ. Sci. Technol. Lett., 6, 413–417, https://doi.org/10.1021/acs.estlett.9b00308, 2019.

Liu, T. and Abbatt, J. P. D.: Oxidation of sulfur dioxide by nitrogen dioxide accelerated at the interface of deliquesced aerosol particles, Nat. Chem., 13, 1173–1177, https://doi.org/10.1038/s41557-021-00777-0, 2021.

Martins-Costa, M. T. C., Anglada, J. M., Francisco, J. S., and Ruiz-López, M. F.: The Aqueous Surface as an Efficient Transient Stop for the Reactivity of Gaseous NO_2 in Liquid Water, J. Am. Chem. Soc., 142, 20937–20941, https://doi.org/10.1021/jacs.0c10364, 2020.

Masoud, C. G. and Ruiz, L. H.: Chlorine-Initiated Oxidation of α-Pinene: Formation of Secondary Organic Aerosol and Highly Oxygenated Organic Molecules, ACS Earth Space Chem., 5, 2307–2319, https://doi.org/10.1021/acsearthspacechem.1c00150, 2021.

McDuffie, E. E., Fibiger, D. L., Dubé, W. P., Lopez-Hilfiker, F., Lee, B. H., Thornton, J. A., Shah, V., Jaeglé, L., Guo, H., and Weber, R. J.: Heterogeneous N_2O_5 uptake during winter: Aircraft measurements during the 2015 WINTER campaign and critical evaluation of current parameterizations, J. Geophys. Res.-Atmos., 123, 4345–4372, 2018.

Miao, R., Chen, Q., Zheng, Y., Cheng, X., Sun, Y., Palmer, P. I., Shrivastava, M., Guo, J., Zhang, Q., Liu, Y., Tan, Z., Ma, X., Chen, S., Zeng, L., Lu, K., and Zhang, Y.: Model bias in simulating major chemical components of $PM_{2.5}$ in China, Atmos. Chem. Phys., 20, 12265–12284, https://doi.org/10.5194/acp-20-12265-2020, 2020.

Pandit, S., Mora Garcia, S. L., and Grassian, V. H.: HONO Production from Gypsum Surfaces Following Exposure to NO_2 and HNO_3: Roles of Relative Humidity and Light Source, Environ. Sci. Technol., 55, 9761–9772, https://doi.org/10.1021/acs.est.1c01359, 2021.

Peng, X., Wang, T., Wang, W., Ravishankara, A. R., George, C., Xia, M., Cai, M., Li, Q., Salvador, C. M., Lau, C., Lyu, X., Poon, C. N., Mellouki, A., Mu, Y., Hallquist, M., Saiz-Lopez, A., Guo, H., Herrmann, H., Yu, C., Dai, J., Wang, Y., Wang, X., Yu, A., Leung, K., Lee, S., and Chen, J.: Photodissociation of particulate nitrate as a source of daytime tropospheric Cl2, Nat. Commun., 13, 939, https://doi.org/10.1038/s41467-022-28383-9, 2022.

Priestley, M., le Breton, M., Bannan, T. J., Worrall, S. D., Bacak, A., Smedley, A. R. D., Reyes-Villegas, E., Mehra, A., Allan, J.,

Webb, A. R., Shallcross, D. E., Coe, H., and Percival, C. J.: Observations of organic and inorganic chlorinated compounds and their contribution to chlorine radical concentrations in an urban environment in northern Europe during the wintertime, Atmos. Chem. Phys., 18, 13481–13493, https://doi.org/10.5194/acp-18-13481-2018, 2018.

Qiu, X., Ying, Q., Wang, S., Duan, L., Wang, Y., Lu, K., Wang, P., Xing, J., Zheng, M., and Zhao, M.: Significant impact of heterogeneous reactions of reactive chlorine species on summertime atmospheric ozone and free-radical formation in north China, Sci. Total Environ., 693, 133580, https://doi.org/10.1016/j.scitotenv.2019.133580, 2019a.

Qiu, X., Ying, Q., Wang, S., Duan, L., Zhao, J., Xing, J., Ding, D., Sun, Y., Liu, B., Shi, A., Yan, X., Xu, Q., and Hao, J.: Modeling the impact of heterogeneous reactions of chlorine on summertime nitrate formation in Beijing, China, Atmos. Chem. Phys., 19, 6737–6747, https://doi.org/10.5194/acp-19-6737-2019, 2019b.

Riva, M., Healy, R. M., Flaud, P.-M., Perraudin, E., Wenger, J. C., and Villenave, E.: Gas- and Particle-Phase Products from the Chlorine-Initiated Oxidation of Polycyclic Aromatic Hydrocarbons, J. Phys. Chem. A, 119, 11170–11181, https://doi.org/10.1021/acs.jpca.5b04610, 2015.

Saiz-Lopez, A. and von Glasow, R.: Reactive halogen chemistry in the troposphere, Chem. Soc. Rev., 41, 6448–6472, 2012.

Seinfeld, J. H. and Pandis, S. N. J. I., New York: Atmospheric chemistry and physics: From air pollution to climate change, John Willey & Sons, ISBN 978-0471720188, 2006.

Su, B., Wang, T., Zhang, G., Liang, Y., Lv, C., Hu, Y., Li, L., Zhou, Z., Wang, X., and Bi, X.: A review of atmospheric aging of sea spray aerosols: Potential factors affecting chloride depletion, Atmos. Environ., 43, 119365, https://doi.org/10.1016/j.atmosenv.2022.119365, 2022.

Tan, F., Tong, S., Jing, B., Hou, S., Liu, Q., Li, K., Zhang, Y., and Ge, M.: Heterogeneous reactions of NO_2 with $CaCO_3$–$(NH_4)_2SO_4$ mixtures at different relative humidities, Atmos. Chem. Phys., 16, 8081–8093, https://doi.org/10.5194/acp-16-8081-2016, 2016.

Tang, B. and Li, Z.: Reaction between a NO_2 Dimer and Dissolved SO_2: A New Mechanism for $ONSO_3^-$ Formation and its Fate in Aerosol, J. Phys. Chem. A, 125, 8468–8475, https://doi.org/10.1021/acs.jpca.1c06215, 2021.

Trebs, I., Bohn, B., Ammann, C., Rummel, U., Blumthaler, M., Königstedt, R., Meixner, F. X., Fan, S., and Andreae, M. O.: Relationship between the NO_2 photolysis frequency and the solar global irradiance, Atmos. Meas. Tech., 2, 725–739, https://doi.org/10.5194/amt-2-725-2009, 2009.

Wang, D. S. and Hildebrandt Ruiz, L.: Chlorine-initiated oxidation of n-alkanes under high-NO_x conditions: insights into secondary organic aerosol composition and volatility using a FIGAERO–CIMS, Atmos. Chem. Phys., 18, 15535–15553, https://doi.org/10.5194/acp-18-15535-2018, 2018.

Wang, D. S. and Ruiz, L. H.: Secondary organic aerosol from chlorine-initiated oxidation of isoprene, Atmos. Chem. Phys., 17, 13491–13508, https://doi.org/10.5194/acp-17-13491-2017, 2017.

Wang, G., Zhang, R., Gomez, M. E., Yang, L., Zamora, M. L., Hu, M., Lin, Y., Peng, J., Guo, S., and Meng, J.: Persistent sulfate formation from London Fog to Chinese haze, P. Natl. Acad. Sci. USA, 113, 13630–13635, 2016.

Wang, J., Li, J., Ye, J., Zhao, J., Wu, Y., Hu, J., Liu, D., Nie, D., Shen, F., and Huang, X.: Fast sulfate formation from oxidation of SO_2 by NO_2 and HONO observed in Beijing haze, Nat. Commun., 11, 1–7, 2020.

Wang, Y., Riva, M., Xie, H., Heikkinen, L., Schallhart, S., Zha, Q., Yan, C., He, X.-C., Peräkylä, O., and Ehn, M.: Formation of highly oxygenated organic molecules from chlorine-atom-initiated oxidation of alpha-pinene, Atmos. Chem. Phys., 20, 5145–5155, https://doi.org/10.5194/acp-20-5145-2020, 2020.

Weis, D. D. and Ewing, G. E.: The Reaction of Nitrogen Dioxide with Sea Salt Aerosol, J. Phys. Chem. A, 103, 4865–4873, https://doi.org/10.1021/jp984488q, 1999.

Xie, X., Hu, J., Qin, M., Guo, S., Hu, M., Wang, H., Lou, S., Li, J., Sun, J., Li, X., Sheng, L., Zhu, J., Chen, G., Yin, J., Fu, W., Huang, C., and Zhang, Y.: Modeling particulate nitrate in China: Current findings and future directions, Environ. Int., 166, 107369, https://doi.org/10.1016/j.envint.2022.107369, 2022.

Xie, Y., Wang, G., Wang, X., Chen, J., Chen, Y., Tang, G., Wang, L., Ge, S., Xue, G., Wang, Y., and Gao, J.: Nitrate-dominated $PM_{2.5}$ and elevation of particle pH observed in urban Beijing during the winter of 2017, Atmos. Chem. Phys., 20, 5019–5033, https://doi.org/10.5194/acp-20-5019-2020, 2020.

Xu, W., Kuang, Y., Zhao, C., Tao, J., Zhao, G., Bian, Y., Yang, W., Yu, Y., Shen, C., Liang, L., Zhang, G., Lin, W., and Xu, X.: NH_3-promoted hydrolysis of NO_2 induces explosive growth in HONO, Atmos. Chem. Phys., 19, 10557–10570, https://doi.org/10.5194/acp-19-10557-2019, 2019.

Yabushita, A., Enami, S., Sakamoto, Y., Kawasaki, M., Hoffmann, M., and Colussi, A.: Anion-catalyzed dissolution of NO_2 on aqueous microdroplets, J. Phys. Chem. A, 113, 4844–4848, 2009.

Yang, J., Li, L., Wang, S., Li, H., Francisco, J. S., Zeng, X. C., and Gao, Y.: Unraveling a New Chemical Mechanism of Missing Sulfate Formation in Aerosol Haze: Gaseous NO_2 with Aqueous HSO_3^- / SO_3^{2-}, J. Am. Chem. Soc., 141, 19312–19320, https://doi.org/10.1021/jacs.9b08503, 2019.

Yao, X. and Zhang, L.: Chemical processes in sea-salt chloride depletion observed at a Canadian rural coastal site, Atmos. Environ., 46, 189–194, 2012.

Yao, X., Fang, M., and Chan, C. K.: The size dependence of chloride depletion in fine and coarse sea-salt particles, Atmos. Environ., 37, 743–751, https://doi.org/10.1016/S1352-2310(02)00955-X, 2003.

Ye, C., Zhang, N., Gao, H., and Zhou, X.: Photolysis of Particulate Nitrate as a Source of HONO and NO_x, Environ. Sci. Technol., 51, 6849–6856, https://doi.org/10.1021/acs.est.7b00387, 2017.

Young, C. J., Washenfelder, R. A., Edwards, P. M., Parrish, D. D., Gilman, J. B., Kuster, W. C., Mielke, L. H., Osthoff, H. D., Tsai, C., Pikelnaya, O., Stutz, J., Veres, P. R., Roberts, J. M., Griffith, S., Dusanter, S., Stevens, P. S., Flynn, J., Grossberg, N., Lefer, B., Holloway, J. S., Peischl, J., Ryerson, T. B., Atlas, E. L., Blake, D. R., and Brown, S. S.: Chlorine as a primary radical: evaluation of methods to understand its role in initiation of oxidative cycles, Atmos. Chem. Phys., 14, 3427–3440, https://doi.org/10.5194/acp-14-3427-2014, 2014.

Yu, C., Wang, Z., Ma, Q., Xue, L., George, C., and Wang, T.: Measurement of heterogeneous uptake of NO_2 on inorganic parti-

cles, sea water and urban grime, J. Environ. Sci., 106, 124–135, https://doi.org/10.1016/j.jes.2021.01.018, 2021.

Zhang, K. and Parker, K. M.: Halogen Radical Oxidants in Natural and Engineered Aquatic Systems, Environ. Sci. Technol., 52, 9579–9594, https://doi.org/10.1021/acs.est.8b02219, 2018.

Zhang, R., Gen, M., Huang, D., Li, Y., and Chan, C. K.: Enhanced Sulfate Production by Nitrate Photolysis in the Presence of Halide Ions in Atmospheric Particles, Environ. Sci. Technol., 54, 3831–3839, https://doi.org/10.1021/acs.est.9b06445, 2020.

Zhang, R., Gen, M., Fu, T.-M., and Chan, C. K.: Production of formate via oxidation of glyoxal promoted by particulate nitrate photolysis, Environ. Sci. Technol., 55, 5711–5720, 2021.

Zhang, R., Gen, M., Liang, Z., Li, Y. J., and Chan, C. K.: Photochemical Reactions of Glyoxal during Particulate Ammonium Nitrate Photolysis: Brown Carbon Formation, Enhanced Glyoxal Decay, and Organic Phase Formation, Environ. Sci. Technol., 56, 1605–1614, https://doi.org/10.1021/acs.est.1c07211, 2022.

Zhang, X., Zhang, Y., Liu, Y., Zhao, J., Zhou, Y., Wang, X., Yang, X., Zou, Z., Zhang, C., Fu, Q., Xu, J., Gao, W., Li, N., and Chen, J.: Changes in the SO_2 Level and PM2.5 Components in Shanghai Driven by Implementing the Ship Emission Control Policy, Environ. Sci. Technol., 53, 11580–11587, https://doi.org/10.1021/acs.est.9b03315, 2019.

Zheng, B., Tong, D., Li, M., Liu, F., Hong, C., Geng, G., Li, H., Li, X., Peng, L., Qi, J., Yan, L., Zhang, Y., Zhao, H., Zheng, Y., He, K., and Zhang, Q.: Trends in China's anthropogenic emissions since 2010 as the consequence of clean air actions, Atmos. Chem. Phys., 18, 14095–14111, https://doi.org/10.5194/acp-18-14095-2018, 2018.